CHINA FOUNDRY Research & Development
Vol. 21 No. 1 January 2024
www.springer.com/41230
https://doi.org/10.1007/s41230-024-2145-7

Thermal and mechanical behavior of casting copper alloy wheel during wheel and belt continuous casting process

Kun Gao and *Yan Peng
School of Mechanical Engineering, Yanshan University, Qinhuangdao 066004, Hebei, China

Abstract: To investigate the thermal and mechanical behavior of casting wheel, a two-dimensional thermo-elastic-plastic finite element model was used to predict the temperature, stress and distortion distribution of the casting wheel during the wheel and belt continuous casting process. The effects of grinding thickness and casting speed on the thermal and mechanical behaviors of the center of the hot face of the casting wheel were discussed in detail. In each rotation, the casting wheel passes through four different spray zones. The results show that the temperature distribution of the casting wheel in different spray zones is similar, the temperature of the hot face is the highest and the temperature reaches the peak in the spray zone III. The stress and distortion depend on the temperature distribution, and the maximum stress and distortion of the hot face are 358.2 MPa and 1.82 mm, respectively. The temperature at the center of the hot face decreases with increasing grinding thickness and increases with increasing casting speed.

Keywords: casting wheel; finite element model; grinding thickness; casting speed; hot face; spray zones

CLC numbers: TP391.9 **Document code:** A **Article ID:** 1672-6421(2024)01-082-09

1 Introduction

The wheel and belt continuous casting process, represented by the continuous Properzi technology [1] and the Southwire Continuous Rod (SCR) technology [2], is an important method for producing copper cast ingot and aluminum cast ingot. The flexible spray water system makes the molten metal in the casting wheel solidify faster, so this process is more energy-saving and efficient. The casting wheel made of copper alloy is the key component of the wheel and belt continuous casting machine, which is important for the production continuity. However, considering the poor working conditions and mechanical damage, the casting wheel, as the mold of the wheel and belt continuous caster, needs to be repaired frequently.

A large number of studies have analyzed the thermal and mechanical behavior of the molds during the continuous casting process by various mathematical models. The complex physical phenomena in the molds, such as the movement of the slag layers [3-5] and the evolution of air gap [6-8], were often simplified to ensure the stability of the calculation process. Samarasekera et al. [9-10] calculated the thermal deformation behavior of the mold through a heat transfer model coupled with a three-dimensional (3-D) elastic-plastic model. They found that the main factors that cause permanent deformation of the mold wall were wall thickness, cooling water velocity, and the position of the mold tube constraint relative to the meniscus level. O`Connor et al. [11] developed a two dimensional (2-D) elastic-plastic model of thin-slab mold which included the effect of creep, the model predicted locations and time to failure of the mold. Thomas et al. [12] thought that the detrimental residual stress and strain of mold can be reduced by optimizing the locations of water slots and small bolt holes based on the 3-D thermo-elastic-plastic creep model. Park et al. [13-14] applied the above mathematical model to study the heat flux and the effects of mold shape on distortion and cracking of the thin-slab mold, their calculations match the plant observations. Xu et al. [15] and Luo et al. [16] analyzed the temperature, stress, distortion of beam blank mold through 2-D thermo-elastic-plastic creep finite element models, a new water slot design for the mold was provided. Moro et al. [17] adopted different

***Yan Peng**
Male, born in 1971, Ph. D, Professor. His research interests mainly focus on intelligent technology of rolling equipment.
E-mail: pengyan@ysu.edu.cn
Received: 2022-10-18; Accepted: 2023-08-18

non-linear material models to simulate the thermo-mechanical behavior of the mold under alternating hot and cold cycles. Chakraborty et al. [18] considered the effect of turbulent flow in the thermo-mechanical model, the most appropriate taper value of the mold was determined. Zeng et al. [19] compared the distortion trend of bloom tube mold under different water pressures in the continuous casting process.

The above studies have focused on vertical molds with water slot cooling in conventional continuous casting process. So far, relatively little effort has been invested to understand the wheel and belt continuous casting process, especially the thermo-mechanical behavior of the casting wheel. Li et al. [20] and Cheung et al. [21] investigated the transient thermal resistance at the metal/casting wheel interface. Åberg et al. [22-23] used the temperature data collected at different positions of the industrial casting wheel as the boundary conditions to simulate the solidification process of the cast ingot. However, previous works have ignored the heat transfer and distortion behavior of the casting wheel. To improve the quality of the cast ingot and extend the service life of the casting wheel, it is necessary to clarify the heat transfer and distortion behavior of the casting wheel.

In the current study, the material of the casting wheel was Cu-Cr-Zr copper alloy, which is widely used in different molds due to its excellent thermal conductivity and corrosion resistance. A 2-D thermo-elastic-plastic model was used to calculate the temperature, stress, and distortion of the casting wheel during the wheel and belt continuous casting process. The boundary conditions of the heat transfer model in different spray zones were emphasized. This work provides theoretical guidance for process design by analyzing the effects of grinding thickness and casting speed on the hot face center.

2 Model description

2.1 Process description and main assumptions

Figure 1 shows the schematic of the wheel and belt casting process. The molten metal was poured from tundish into a mold consisting of a grooved wheel and an endless steel belt, and the casting wheel rotates continuously on its axis. The outer walls of the casting wheel and steel belt were cooled with spray water. The water cooling system consists of four spray zones in order to ensure flexibility in the adjustment of the water flow. Spray zones I and II play an important role in the successful solidification of the cast ingot. The function of spray zones III and IV is to ensure the initial rolling temperature of the cast ingot before it enters the rolling mill and to prevent the abnormal local temperature in the casting wheel. Finally, the fully solidified cast ingot with a trapezoidal transverse section was pulled out as the casting wheel rotated to a certain angle.

A typical casting wheel and the key dimensions of the cross-section are shown in Fig. 2. The diameter of the casting wheel was about 2.5 m, and it took about 45 s for each rotation. The material of the casting wheel was Cu-Cr-Zr copper alloy, which contains 0.65% Cr and 0.1% Zr, and balance copper. After a period of service, the inner surface of the casting wheel needs to be ground for further use to prevent material wastage. The grinding thickness was 0, 5, 10, 15 mm. The arrangement of the nozzles in different spray zones is illustrated in Fig. 3. There was no spray water on the operation side and machine side in the spray zone I and spray zone II. All walls of the casting wheel were cooled by spray water in the spray zone III and spray zone IV. The water flow of each spray zone is controlled by different cooling water branch pipes, and the water flow increases continuously from spray zone I to spray zone IV.

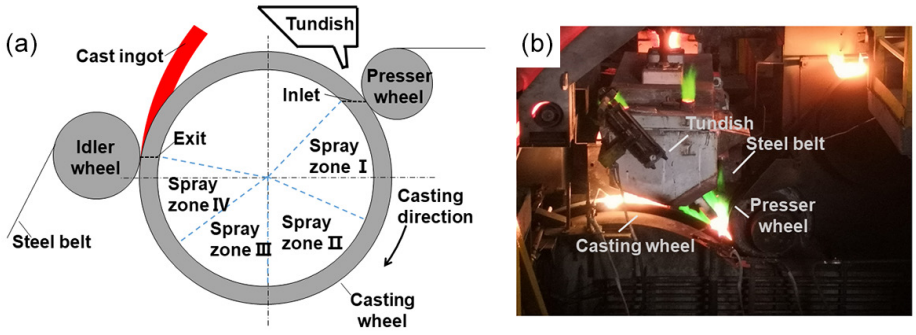

Fig. 1: Schematic of wheel and belt casting process (a) and industrial process (b)

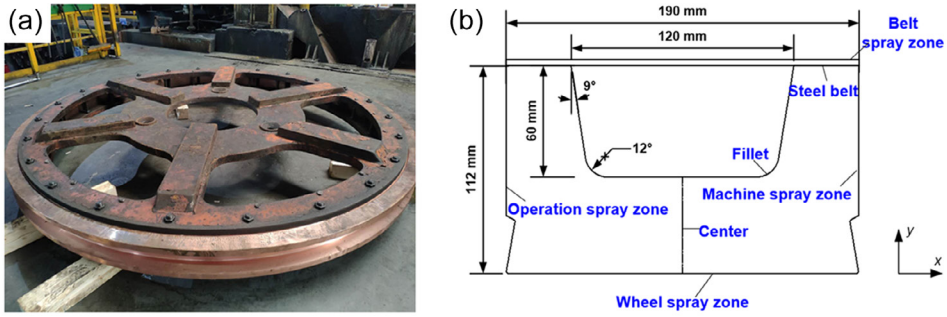

Fig. 2: A typical casting wheel (a) and schematic of casting wheel cross-section (b)

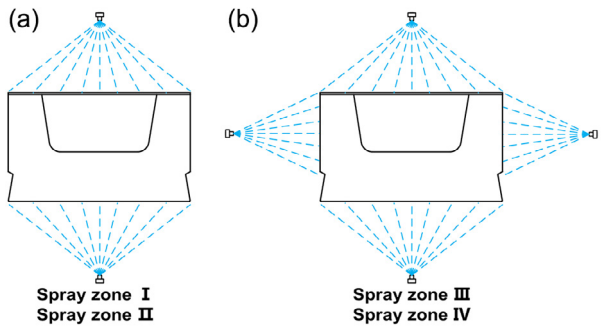

Fig. 3: Arrangement of spray nozzles in spray zones I and II (a), spray zones III and IV (b)

To improve the computational efficiency, the following assumptions were made during the calculation: (1) the heat transfer process in the casting direction was ignored; (2) the friction and tangential forces generated by the metal fluid were not considered; (3) the material of the casting wheel was isotropic, the physical properties of each tiny unit of the object were the same, the elastic constants, Poisson's ratio did not change with location; (4) the effects of creep of mold were negligible.

2.2 Heat flow model

A 2-D transient heat transfer model was used to describe the thermal behavior of the casting wheel in the spray zone. Based on the law of conservation of energy [24], the heat transfer model in a rectangular Cartesian coordinate system can be described as:

$$\rho_M c_M \frac{\partial T_M}{\partial \tau} = \frac{\partial}{\partial x}\left(k_M \frac{\partial T_M}{\partial x}\right) + \frac{\partial}{\partial y}\left(k_M \frac{\partial T_M}{\partial y}\right) \quad (1)$$

where ρ_M is the density of copper alloy, kg·m^{-3}, c_M is the heat capacity of copper alloy, J·kg^{-1}·°C^{-1}, k_M is the thermal conductivity of copper alloy, W·m^{-1}·°C^{-1}, T_M is the temperature of the casting wheel, °C. The density, thermal conductivity, specific heat capacity, and thermal expansion coefficient of the material are related to the temperature, as shown in Fig. 4.

To avoid damage of the casting wheel by the high-temperature molten metal, the casting wheel needed to be preheated and the initial temperature was set to 120 °C. The heat flux at the hot face in the spray cooling zone could be determined from the following empirical expression [22]:

$$q = 4.41e^{-(((t-22.92)/4.505)^2)} + 3.199e^{-(((t-3.71)/2.645)^2)} + 3.157e^{-(((t-12.52)/7.657)^2)} \quad (2)$$

where $t=z/v_c$, z represents the distance from the inlet, m, v_c is the casting speed, m·s^{-1}.

Spray cooling is a type of forced convection, which offers the advantages of high cooling efficiency. For calculating the convective heat transfer coefficient, h_w, Eq. (3) is obtained from Wendelstorf's [25] experimental data:

$$h_w = 190 + \tanh\left(\frac{V_s}{8}\right) \times \left(140 \cdot V_s \left[1 - \frac{V_s \cdot \Delta T}{72000}\right] + 3.26 \cdot \Delta T^2 \left\{1 - \tanh\left(\frac{\Delta T}{128}\right)\right\}\right) \quad (3)$$

where $\Delta T=T_s-T_w$, T_w is the temperature of spray cooling water, °C; T_s is the temperature of the outer wall of the casting wheel, °C; V_s is the spray water mass flux, kg·m^{-2}·s^{-1}.

Beyond the spray zones, the heat is mainly taken away by air convection and heat radiation. Based on Newton's law of cooling, the convection boundary condition can be given as:

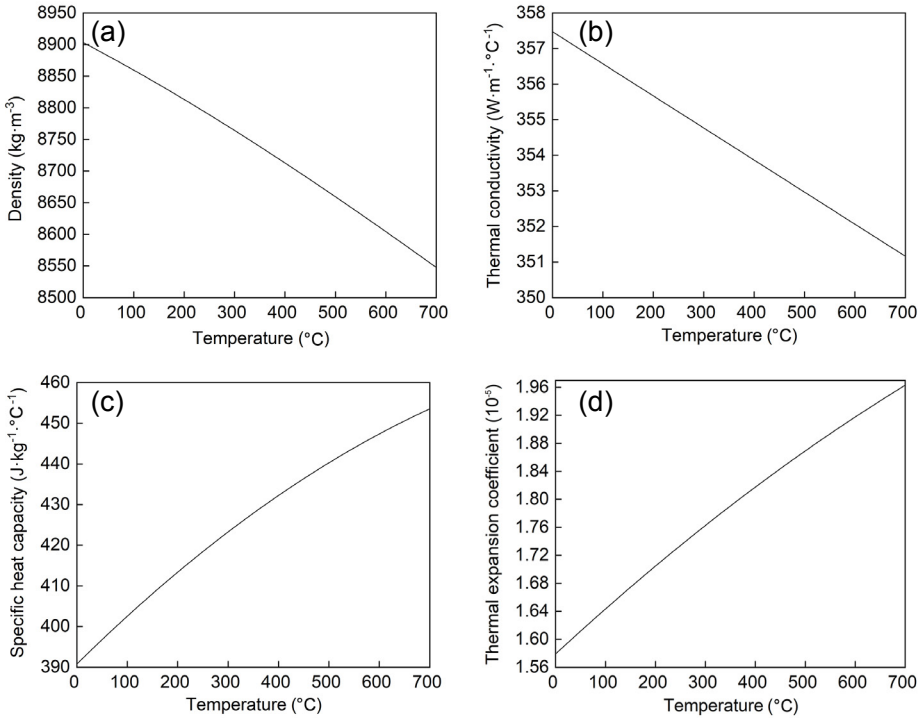

Fig. 4: Material properties of Cu-Cr-Zr copper alloy related to temperature: (a) density; (b) thermal conductivity; (c) specific heat capacity; (d) thermal expansion coefficient

$$q = h_T(T_s - T_a) \tag{4}$$

with

$$h_T = h_a + h_{rad} \tag{5}$$

where T_a is the ambient temperature, °C; the natural convection heat transfer coefficient, h_a, and radiation heat transfer coefficient, h_{rad}, are calculated by Eqs. (6) and (7), respectively.

$$h_a = \frac{k_a}{l}\left(0.68 + \frac{0.67Ra^{1/4}}{\left(1+((0.492k_a)/(\mu_a c_a))^{9/16}\right)^{4/9}}\right) \tag{6}$$

$$h_{rad} = \sigma\varepsilon[(T_s+273)+(T_a+273)][(T_s+273)^2+(T_a+273)^2] \tag{7}$$

where k_a is the air thermal conductivity, W·m^{-1}·°C^{-1}; l is the feature size, m; Ra is the Rayleigh number; μ_a is the air viscosity, kg·m^{-1}·s^{-1}; c_a is the air heat capacity, J·kg^{-1}·°C^{-1}; σ is the Stefan-Boltzman constant; ε is the emissivity of the casting wheel.

2.3 Stress model

Displacement, strain, and stress are calculated by solving the standard equilibrium equation [Eq. (8)] [12]:

$$\nabla \cdot \boldsymbol{S} + \boldsymbol{F} = 0 \tag{8}$$

where $\boldsymbol{S}$ is the stress tensor, $\boldsymbol{F}$ is the mass force. The temperature field can be used as the thermal load for stress model.

Plastic deformation occurs when the equivalent stress exceeds the initial yield stress, and the yield stress is related to temperature, as shown in Table 1 [26]. The casting wheel is more prone to plastic deformation when serving in a high-temperature environment. Therefore, plasticity needs to be considered during the calculation of thermal stress. The total strain tensor is computed by Eq. (9):

$$\boldsymbol{\varepsilon}^{total} = \boldsymbol{\varepsilon}^{el} + \boldsymbol{\varepsilon}^{pl} + \boldsymbol{\varepsilon}^{th} \tag{9}$$

where $\boldsymbol{\varepsilon}^{el}$ is the elastic strain tensor, $\boldsymbol{\varepsilon}^{pl}$ is the plastic strain tensor, and $\boldsymbol{\varepsilon}^{th}$ is the thermal strain tensor. In the elastic region, the elastic strain tensor and the stress tensor are related through Hook's law. In the plastic region, the Von Mises yield criterion is used to describe the relationship between the plastic strain tensor and the stress tensor [18]. The thermal strain is calculated by Eq. (10). The displacement and strain are correlated by the compatibility equation [Eq. (11)].

$$\boldsymbol{\varepsilon}^{th} = \alpha\Delta T_r \cdot \boldsymbol{I} \tag{10}$$

$$\boldsymbol{\varepsilon}^{total} = \frac{1}{2}\left[\left(\nabla \boldsymbol{u}\right)^T + \left(\nabla \boldsymbol{u}\right)\right] \tag{11}$$

where α is the thermal expansion coefficient, as shown in Fig. 4(d), ΔT_r is the difference between the temperature at each position of the casting wheel and the reference temperature, $\boldsymbol{I}$ is the identity matrix, and $\boldsymbol{u}$ is the displacement vector.

Table 1: Yield stress of Cu-Cr-Zr copper alloy [26]

Temperature (°C)	0	20	200	350	500	600
Yield stress (MPa)	300	300	280	240	165	130

The load and displacement conditions of the casting wheel were set, as shown in Fig. 5, the hot face is mainly affected by the hydrostatic pressure. The calculated expression for hydrostatic pressure is given by $P=\rho_c gh$, where ρ_c is the density of the cast ingot, kg·m^{-3}; g is the acceleration of gravity, m·s^{-2}; h is the vertical distance from the inlet, m.

The top walls of the casting wheel are mainly subjected to the pressure generated by the steel belt. The pressure distribution in this part is assumed to be uniform and does not change with the rotation position of the casting wheel; the uniform pressure is 3,000 Pa. The bottom walls of the casting wheel are constrained by the support equipment and do not move, the displacement boundary condition of this part is set as fixed constraint, and boundary conditions are:

$$u_x = 0, \quad u_y = 0 \tag{12}$$

The operating conditions and thermal properties of materials are listed in Table 2.

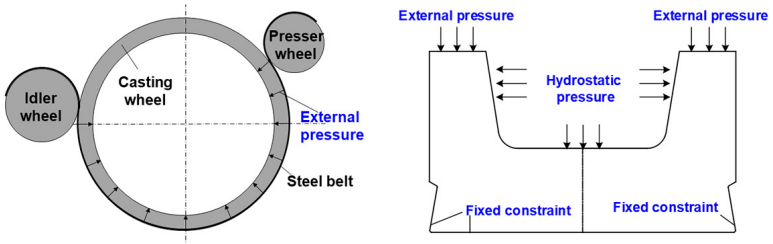

Fig. 5: Mechanical boundary conditions

Table 2: Operating conditions and thermal properties of materials

Parameter	Value	Parameter	Value
Temperature of spray cooling water, T_w (°C)	20	Air heat capacity, c_a (J·kg^{-1}·°C^{-1})	1,004
Ambient temperature, T_a (°C)	25	Emissivity of casting wheel, ε	0.4
Air thermal conductivity, k_a (W·m^{-1}·°C^{-1})	0.026	Water heat capacity, c_w (J·kg^{-1}·°C^{-1})	4,200
Air viscosity, μ_a (kg·m^{-1}·s^{-1})	1.8×10^{-5}	Water density, ρ_w (kg·m^{-3})	1,000

3 Results and discussion

3.1 Validation of model

To verify the correctness of the model, the measured and calculated values of the average heat flux were compared. The measured value is calculated by Eq. (13):

$$\bar{q}_w = \frac{c_w \rho_w W (T_{ow} - T_w)}{A} \quad (13)$$

where c_w is the water heat capacity, J·kg^{-1}·℃$^{-1}$; ρ_w is the water density, kg·m^{-3}; W is water flow rate, m^3·s^{-1}; T_{ow} is the output temperature of spray water, ℃; A is the exposed mold face area, m^2.

The temperature of the spray water in each spray zone needs to be counted before and after cooling. The same verification method was also applied by Park [13] and Du [27], and they found that the average error between their calculated and measured values is less than 10%, which is considered acceptable. In this study, the calculated value is very close to the measured value with an average error of 6.9%, as shown in Fig. 6. This error is caused by the instability of the collection temperature process, thus the model can be considered reasonable.

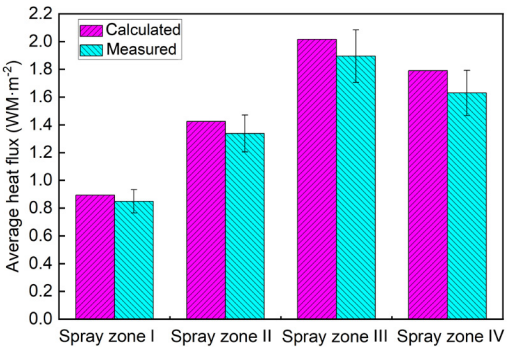

Fig. 6: Comparison of measured and calculated average heat flux of different spray zones

3.2 Temperature, stress and distortion distributions of cross-section

In order to describe the development of temperature, stress, and distortion of the casting wheel during the cooling process, a cross-section is extracted in each spray zone, and the calculation results are shown in Figs. 7–9.

In Fig. 7, the temperature distribution trend of each section is almost similar, temperature decreases with increasing the distance from the hot face. Since the hot face of the casting wheel is in direct with the surface of the cast ingot, the temperature of the hot face is significantly higher than in other positions. The temperature in the corner area of the casting wheel is much lower than that at other locations. The main factor contributing to the faster dissipation of heat in the corner area is the fact that the heat transfer occurs in two directions. The non-uniform distribution of temperature tends prone to cause cracks on the surface of the casting wheel.

In the spray zone I and spray zone II, the bottom of the casting wheel is cooled by the spray water, while the operation side and the machine side were only affected by heat radiation and natural convection generated by the air, resulting in lower heat dissipation efficiency and higher temperature. The sharp increase of the spray water flow in the spray zone III makes the cast ingot solidify rapidly and release a large amount of latent heat of solidification [28]. Therefore, the temperature of the cross-section of the casting wheel will briefly reach the peak in the spray zone III. The temperature gradually decreases in the spray zone IV.

Figure 8 shows computed stress on each cross-section of the spray zone. The distribution of stress roughly corresponds to the temperature gradient. In the initial stage of cooling, due to the large temperature gradient in the area near the hot face and the hydrostatic pressure of the metal, the stress is relatively high.

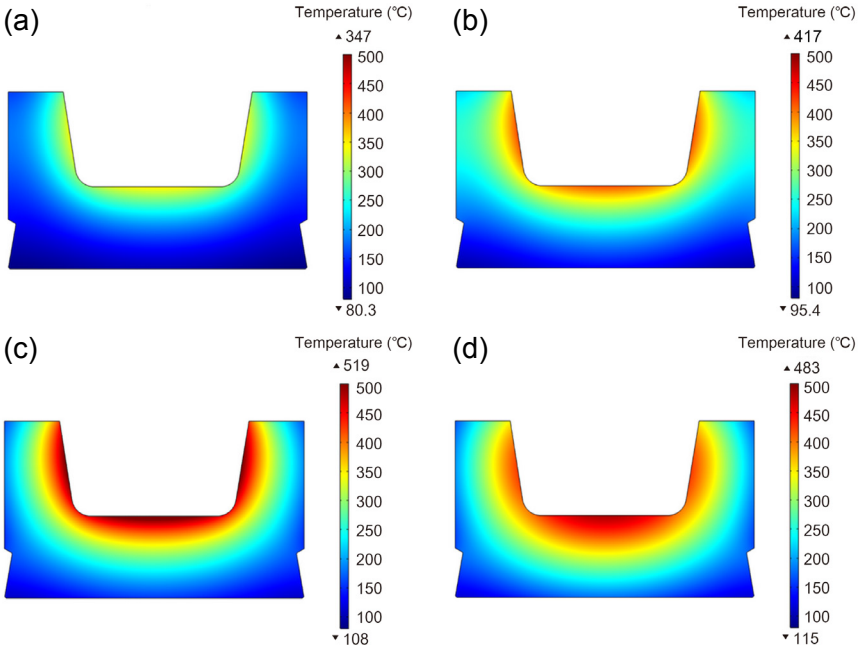

Fig. 7: Temperature fields of casting wheel in spray zone I (a), spray zone II (b), spray zone III (c), and spray zone IV (d)

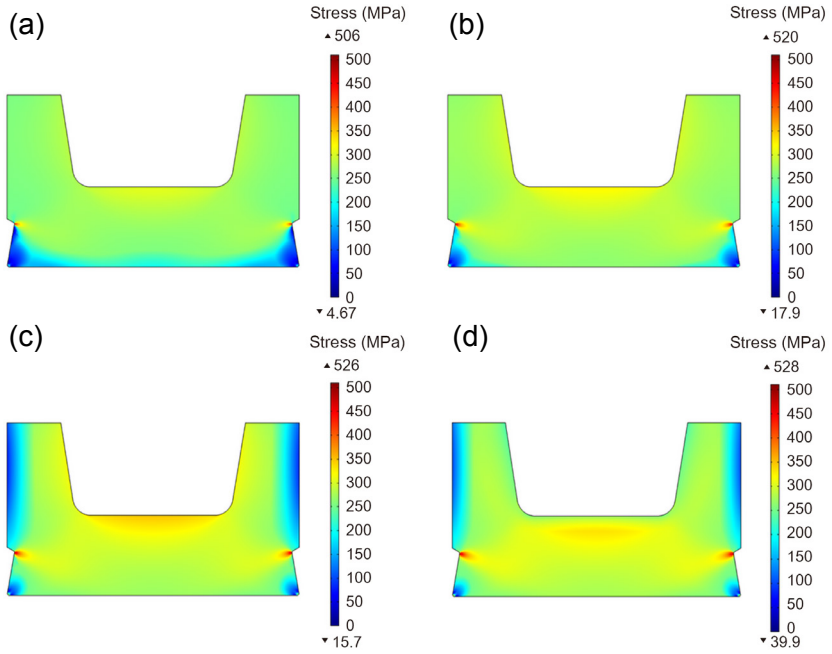

Fig. 8: Stress fields of casting wheel in the spray zone I (a), spray zone II (b), spray zone III (c), and spray zone IV (d)

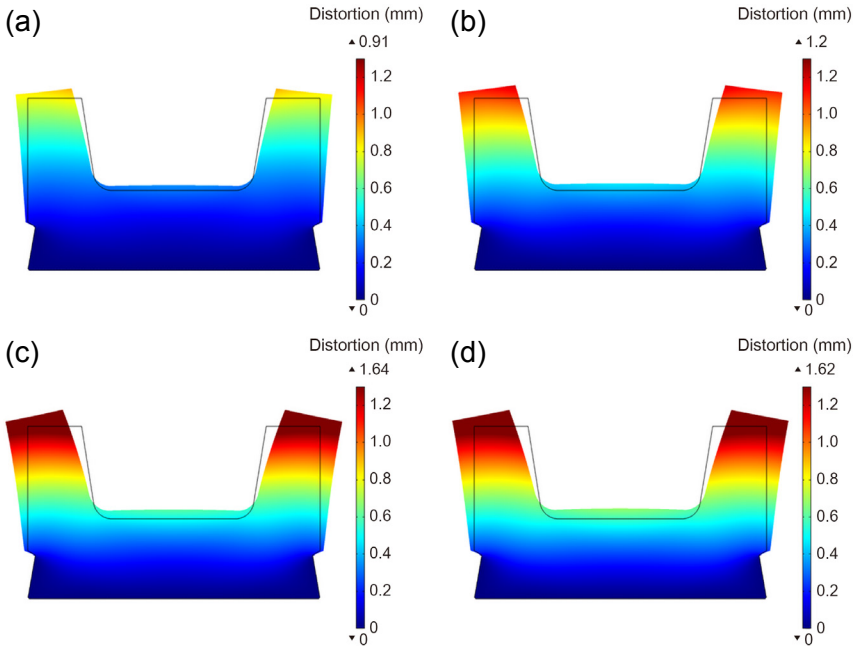

Fig. 9: Distortion fields of casting wheel in spray zone I (a), spray zone II (b), spray zone III (c), and spray zone IV (d)

As the cooling time increases, the heat released from the cast ingot is greatly reduced, the temperature gradient of the hot face is constantly decreased. The hot face is no longer affected by the hydrostatic pressure due to the complete solidification of the cast ingot, and the stress on the hot face is constantly decreased. Moreover, in spray zones III and IV, the stresses on the operation side and machine side are lower due to the lower temperature gradient.

Due to the restraint of the support equipment, the corner attachments of the casting wheel have fixed constraints. The angle of the chamfer is relatively small, stress concentration occurs, and the highest stress is approximately 520 MPa. The stress in this area is greater than the yield stress of the copper alloy, resulting in permanent distortion.

Figure 9 shows the distorted geometries of the cross-section of the casting wheel. Due to the increase in the thermal expansion coefficient with temperature, locations at higher temperatures exhibit more pronounced thermal distortion. Therefore, the large distortion occurs at the hot face of the casting wheel with the highest temperature. Compared with the location with larger wall thickness, the distortion is more serious at the location with smaller wall thickness, and there is a tendency of outward bending. The bottom of the casting wheel is almost not distorted owing to the restraining effect of the support equipment. When the distortion reaches a certain level, there will be an air gap between the steel belt and the casting wheel, resulting in a decrease in cooling efficiency. At the same time, when the steel belt and the casting wheel cannot be closely attached, the danger of molten metal leakage is likely to occur.

3.3 Temperature, stress and distortion distributions of hot face

The state of the hot face of the casting wheel is closely related to the uniformity of the solidification shell of the cast ingot. Meanwhile, the service life of the casting wheel depends on the wear resistance of its hot face. Thus, it is extremely important to analyze the thermo-mechanical behavior of the hot face in different spray zones.

In Fig. 10(a), the temperature of the hot face increases continuously until it reaches a maximum at the end of the spray zone III, and then gradually decreases in the spray zone IV. The highest temperature appears at the center of the hot face, and the temperature at the fillet and edge is relatively low. The temperature at the center of the hot face reaches a peak of about 583 °C at a distance of 3.78 m from the inlet, and the temperature difference between the fillet and the center is 104 °C. In a word, the higher the overall temperature of the hot face, the greater the temperature difference between the fillet and the other locations. The non-uniform cooling of the hot face can be prevented by reasonably optimizing the cooling process parameters of the spray zone. For example, gradually increase the water flow, change the installation position and angle of the nozzle.

In Fig. 10(b), the distribution of equivalent stress on the hot face is similar to the development of temperature. The rapid increase of temperature on the hot face brings a larger temperature gradient, and the stress increases continuously, with a maximum value of 358.2 MPa. The stress around the fillet is kept at a low level, and the radius of the fillet plays a very important role. After the cast ingot is solidified and formed, the latent heat is no longer released, and the temperature gradient near the hot face decreases rapidly as the temperature decreases, thus the thermal stress shows a decreasing trend. Then, there is a significant temperature difference between the hot face and other locations with further cooling, the thermal stress increases again with the increase of temperature gradient.

It is observed in Fig. 10(c) that the degree of distortion of the hot face is also temperature dependent. The center of the hot face is restricted by the pressure of the cast ingot and cannot expand freely to produce large distortion. Since the edges of the hot face are not constrained, the distortion is much larger than in other locations, and the maximum value can reach 1.82 mm.

Although the distortion at the fillet is the lowest, the distortion at other locations and the solidification shrinkage of the cast ingot will cause a large air gap, which could lead to fatal defects in fragile cast ingot corners, as shown in Fig. 11.

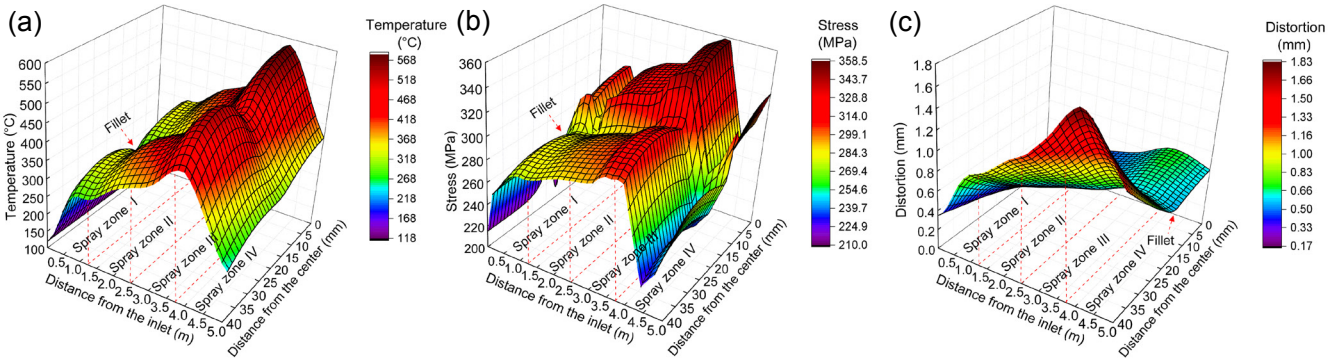

Fig. 10: Temperature (a), stress (b), distortion (c) distribution of the hot face along casting direction

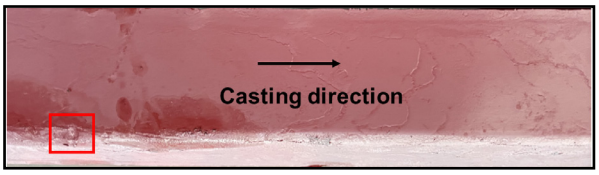

Fig. 11: Defects at fillet of cast ingot

3.4 Effect of grinding thickness on thermal and mechanical behavior of the center of hot face

Some factors can damage the hot face of the casting wheel and produce permanent distortion and cracks, for example, alternately affected by rapid cooling and rapid heating loads during one rotation of the casting wheel, the friction force generated by dragging the ingot will also damage the hot face [29-30]. At the same time, the impact of molten metal on the hot face will aggravate distortion and crack propagation. In addition to reducing the service life of the casting wheel, these cracks also scratch the surface of the cast ingot and destroy its continuity. The adverse effects of distortion and cracks on the quality of cast ingot can be effectively reduced by grinding the hot face of the casting wheel. However, the bottom wall thickness of the casting wheel is required to be greater than 25 mm to prevent local overheating and burn-throug [23].

The thermal behavior of the casting wheel with different grinding thicknesses at a casting speed of 9.7 $m \cdot min^{-1}$ was investigated. Figure 12 shows the profiles of temperature, stress, and distortion at the center of the hot face with different grinding thicknesses. In Fig. 12(a), the trends of the temperature profiles for different grinding thicknesses are similar to each other. With the increase of grinding thickness, the temperature of the hot face decreases continuously, and the temperature difference between the highest temperature without grinding and with the grinding amount of 15 mm is 27 °C. This is mainly because the thinner the thickness of the casting wheel, the lower the thermal resistance, and the heat

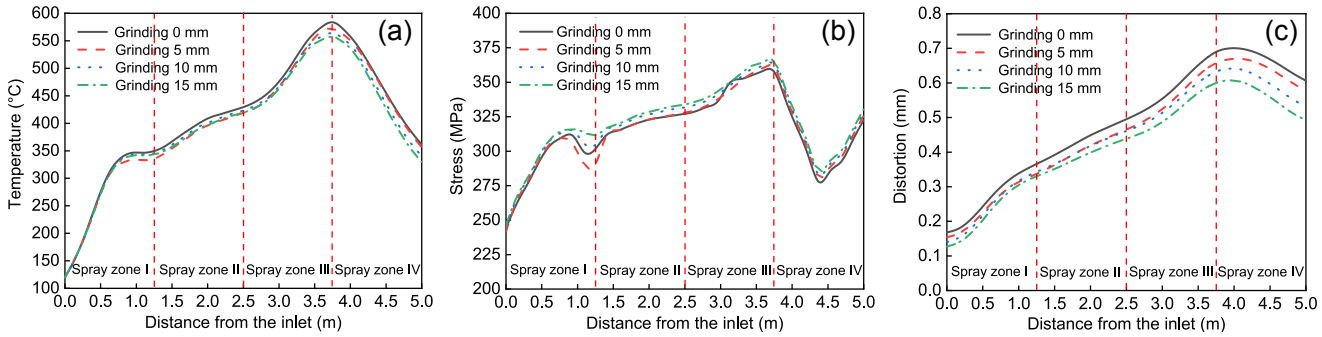

Fig. 12: Profiles of temperature (a), stress (b) and distortion (c) in the center of hot face with different grinding thicknesses during operation

is more easily transferred. In addition, owing to the change in temperature gradient, it can be found that the stress increases slightly as the grinding thickness increases, and the peak stress is still located at the end of the spray zone III. The variation of the distortion is shown in Fig. 12(c), since the thin wall thickness reduces the temperature difference between the hot face and the outer wall, the larger the grinding thickness, the smaller the distortion.

3.5 Effect of casting speed on thermal and mechanical behavior of the center of hot face

In order to discuss the influence of the casting speed, the calculation conditions are exactly the same except for the casting speed. Figure 13(a) compares the temperature at the center of the hot face with different casting speeds. It indicates the higher casting speed leads to higher temperature. The maximum temperature increases from 550 °C to 600 °C as the casting speed improves from 9.1 m·min^{-1} to 10.3 m·min^{-1}. The reason for this trend is that the increase of casting speed shortens the residence time of cast ingot in the casting wheel and lengthens the length of liquid core. The thinner shells make the cast ingot to be more susceptible to expansion and distortion by static pressure, reducing the air gap between the cast ingot and the casting wheel, and increasing heat exchange [31].

In Figs. 13(b) and (c), the stress and distortion in the center of the hot face increase with the increase of casting speed. The maximum stress and maximum distortion are 360.77 MPa and 0.65 mm, 362.89 MPa and 0.70 mm, and 365.32 MPa and 0.72 mm at the casting speeds of 9.1 m·min^{-1}, 9.7 m·min^{-1} and 10.3 m·min^{-1}, respectively. The thermal stress and distortion of the casting wheel arise from the difference in thermal expansion of internal nodes. Permanent distortion of the casting wheel tends to occur in the high temperature region due to the decrease in yield strength. In general, the stress and the distortion are very sensitive to temperature distribution, and are characterized by obvious non-uniformity.

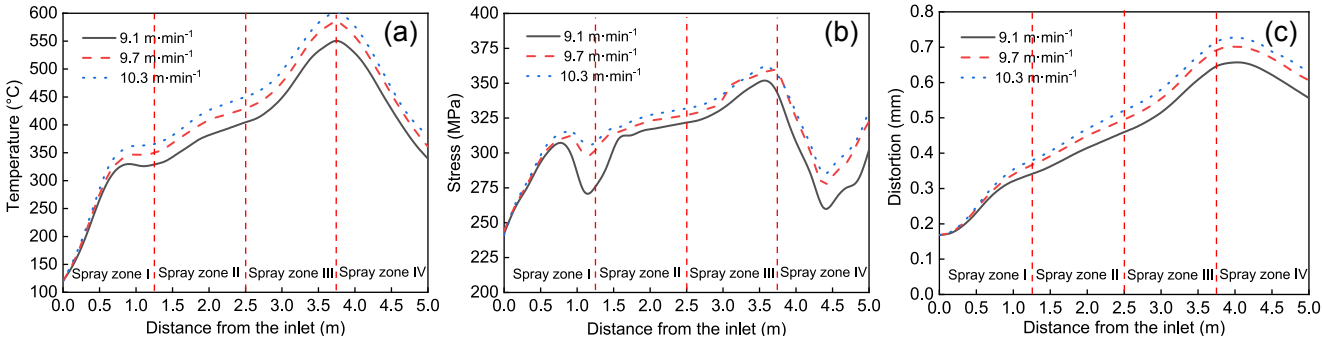

Fig. 13: Profiles of temperature (a), stress (b) and distortion (c) in the center of hot face with different casting speeds during operation

4 Conclusions

The thermal and mechanical behavior of the casting wheel in different spray zones were analyzed based on a 2-D thermo-elastic-plastic model. The effects of different grinding thicknesses and casting speeds on the temperature, stress and distortion of the center of the hot face were compared. The main conclusions are as follows:

(1) The temperature distribution of the casting wheel is not uniform, and the overall temperature of the casting wheel will reach the peak in the spray zone III. The maximum stress is in the corner of the operation side and the machine side due to the restraint of the support equipment. Under the influence of temperature, the distortion of the hot face is the most severe.

(2) The highest temperature of the hot face is concentrated at the center. Because of the two-dimensional heat transfer, the temperature of the fillet and edge is relatively low, and the air gap is easily generated at the fillet.

(3) The wall thickness of the casting wheel becomes thinner and the heat is more easily removed by the spray water, thus

the temperature will keep decreasing with the increase of grinding thickness. The distortion has the same tendency as the temperature.

(4) The increase of the casting speed shortens the cooling time of the cast ingot, the excess heat leads to an increase in the temperature of the casting wheel. The thermal expansion causes the stress and distortion to increase with the increase of temperature.

Acknowledgments

This work was financially supported by the National Natural Science Foundation of China (Grant No. U20A20289), the Innovative Research Groups Project of the Natural Science Foundation of Hebei Province (Grant No. E2021203011), and the Central Government Guides Local Science and Technology Development Fund Project (Grant No. 206Z1601G).

Conflict of interest

The authors declare that they have no conflict of interest.

References

[1] Dablement S, Mortensen D, Fjaer H, et al. Modelling of shrinkage cavity defects during the wheel and belt casting process. IOP Conf. Series: Materials Science and Engineering, 2012, 33: 012056.
[2] Admas R, Sinha U. Improving the quality of continuous copper rod. JOM, 1990, 42(5): 31–34.
[3] Meng Y, Thomas B G. Heat transfer and solidification model of continuous slab casting: CON1D. Metall. Mater. Trans. B, 2003, 34(5): 685–705.
[4] Meng Y, Thomas B G. Modeling transient slag-layer phenomena in the shell mold gap in continuous casting of steel. Metall. Mater. Trans. B, 2003, 34(5): 707–725.
[5] Meng Y, Thomas B G. Simulation of microstructure and behavior of interfacial mold slag layers in continuous casting of steel. ISIJ Int., 2006, 46(5): 660–669.
[6] Vynnycky M. An asymptotic model for the formation and evolution of air gaps in vertical continuous casting. Proc. R. Soc. A, 2009, 465: 1617–1644.
[7] Cai Z Z, Zhu M Y. Non-uniform heat transfer behavior during shell solidification in a wide and thick slab continuous casting mold. Int. J. Miner. Metall. Mater., 2014, 21(3): 240–250.
[8] Niu Z Y, Cai Z Z, Zhu M Y. Dynamic distributions of mold flux and air gap in slab continuous casting mold. ISIJ Int., 2019, 59(2): 283–292.
[9] Samarasekera I V, Brimacombe J K. The thermal field in continuous casting molds. Canadian Metallurgical Quarterly, 1979, 18(3): 251–266.
[10] Samarasekera I V, Anderson D L, Brimacombe J K. The thermal distortion of continuous casting billet molds. Metall. Mater. Trans. B, 1982, 13(1): 91–104.
[11] O`Connor T G, Dantzig J A. Modeling the thin-slab continuous casting mold. Metall. Mater. Trans. B, 1994, 25(3): 443–457.
[12] Thomas B G, Li G, Moitra A, et al. Analysis of thermal and mechanical behavior of copper molds during continuous casting of steel slabs. In: Proceedings of the 80th Steelmaking Conference, Chicago, Illinois, 1997: 1–19.
[13] Park J K, Thomas B G, Samarasekera I V, et al. Thermal and mechanical behavior of copper molds during thin-slab casting (I): Plant trail and mathematical modeling. Metall. Mater. Trans. B, 2002, 33(3): 425–435.
[14] Park J K, Thomas B G, Samarasekera I V, et al. Thermal and mechanical behavior of copper molds during thin-slab casting (II): Mold crack formation. Metall. Mater. Trans. B, 2002, 33(3): 437–449.
[15] Xu H L, Wen G H, Sun W, et al. Thermal behaviour of molds with different water channels and their influence on quality in continuous casting of beam blanks. Ironmaking and Steelmaking, 2010, 37(5): 380–386.
[16] Luo W, Yan B, Lu X, et al. Improvement of water slot design for beam blank casting mold. Ironmaking and Steelmaking, 2013, 40(8): 582–589.
[17] Moro L, Novak J S, Benasciutti D, et al. Thermal distortion in copper molds for continuous casting of steel: Numerical study on creep and plasticity effect. Ironmaking and Steelmaking, 2019, 46(1): 97–104.
[18] Chakraborty S, Ganguly S, Talukdara P. Determination of optimal taper in continuous casting billet mold using thermo-mechanical models of mold and billet. J. Mater. Process. Technol., 2019, 270: 132–141.
[19] Zeng J H, Gan M J, Yan X B, et al. Mathematical modeling of heat transfer and deformation of bloom tube mold in continuous casting process. Metall. Mater. Trans. B, 2020, 51(1): 213–221.
[20] Li G W, Thomas B G. Transient thermal model of the continuous single-wheel thin-strip casting. Metall. Mater. Trans. B, 1996, 27(3): 509–525.
[21] Cheung N, Santos N S, Quaresma J M V, et al. Interfacial heat transfer coefficients and solidification of an aluminum alloy in a rotary continuous caster. Int. J. Heat Mass Transf., 2009, 52(1–2): 451–459.
[22] Åberg J, Vynnycky M, Fredriksson H. Heat-flux measurements of industrial on-site continuous copper casting and their use as boundary conditions for numerical simulations. Trans. Ind. Inst. Met., 2009, 62(4): 443–446.
[23] Åberg J, Vynnycky M, Fredriksson H, et al. An on-site experimental heat flux study and its interpretation in a FEMLAB finite element simulation of continuous casting of copper in the South-Wire process. Trans. Ind. Inst. Met., 2005, 58(4): 509–515.
[24] Chen L Q, Zhao Y H. From classical thermodynamics to phase-field method. Progress in Materials Science, 2022, 124: 1–34.
[25] Wendelstorf J, Spitzer K H, Wendelstorf R. Spray water cooling heat transfer at high temperatures and liquid mass fluxes. Int. J. Heat Mass Transf., 2009, 51(19–20): 4902–4910.
[26] Li G, Thomas B G, Stubbins J F. Modeling creep and fatigue of copper alloys. Metall. Mater. Trans. A, 2000, 31(10): 2491–2502.
[27] Du F M, Wang X D, Liu Y, et al. Investigation on thermo-mechanical behavior of mold corner for continuous casting slab. ISIJ Int., 2015, 55(10): 2150–2157.
[28] Wang H M, Li G R, Lei Y C, et al. Mathematical heat transfer model research for the improvement of continuous casting slab temperature. ISIJ Int., 2005, 45(9): 1291–1296.
[29] Wang X, Zhang S, Yao M, et al. Effect of casting process on mold friction during wide, thick slab continuous casting. Ironmaking and Steelmaking, 2014, 41(6): 464–472.
[30] Odagaki T, Aramaki N, Miki Y. Estimation of lubrication and heat transfer by measurement of friction force in mold. ISIJ Int., 2018, 58(3): 521–526.
[31] Chow C, Samarasekera I V. High speed continuous casting of steel billets: Part 1: General overview. Ironmaking and Steelmaking, 2002, 29(1): 53–59.